Kinetic Modeling of ^{18}F-(2*S*,4*R*)4-Fluoroglutamine in Mouse Models of Breast Cancer to Estimate Glutamine Pool Size as an Indicator of Tumor Glutamine Metabolism

Varsha Viswanath, Rong Zhou, Hsiaoju Lee, Shihong Li, Abigail Cragin, Robert K. Doot, David A. Mankoff, and Austin R. Pantel

Department of Radiology, University of Pennsylvania, Philadelphia, Pennsylvania

The PET radiotracer ^{18}F-(2*S*,4*R*)4-fluoroglutamine (^{18}F-Gln) reflects glutamine transport and can be used to infer glutamine metabolism. Mouse xenograft studies have demonstrated that ^{18}F-Gln uptake correlates directly with glutamine pool size and is inversely related to glutamine metabolism through the glutaminase enzyme. To provide a framework for the analysis of ^{18}F-Gln-PET, we have examined ^{18}F-Gln uptake kinetics in mouse models of breast cancer at baseline and after inhibition of glutaminase. We describe results of the preclinical analysis and computer simulations with the goal of model validation and performance assessment in anticipation of human breast cancer patient studies. **Methods:** Triple-negative breast cancer and receptor-positive xenografts were implanted in athymic mice. PET mouse imaging was performed at baseline and after treatment with a glutaminase inhibitor or a vehicle solution for 4 mouse groups. Dynamic PET images were obtained for 1 h beginning at the time of intravenous injection of ^{18}F-Gln. Kinetic analysis and computer simulations were performed on representative time–activity curves, testing 1- and 2-compartment models to describe kinetics. **Results:** Dynamic imaging for 1 h captured blood and tumor time–activity curves indicative of largely reversible uptake of ^{18}F-Gln in tumors. Consistent with this observation, a 2-compartment model indicated a relatively low estimate of the rate constant of tracer trapping, suggesting that the 1-compartment model is preferable. Logan plot graphical analysis demonstrated late linearity, supporting reversible kinetics and modeling with a single compartment. Analysis of the mouse data and simulations suggests that estimates of glutamine pool size, specifically the distribution volume (V_D) for ^{18}F-Gln, were more reliable using the 1-compartment reversible model than the 2-compartment irreversible model. Tumor-to-blood ratios, a more practical potential proxy of V_D, correlated well with volume of distribution from single-compartment models and Logan analyses. **Conclusion:** Kinetic analysis of dynamic ^{18}F-Gln-PET images demonstrated the ability to measure V_D to estimate glutamine pool size, a key indicator of cellular glutamine metabolism, by both a 1-compartment model and Logan analysis. Changes in V_D with glutaminase inhibition support the ability to assess response to glutamine metabolism-targeted therapy. Concordance of kinetic measures with tumor-to-blood ratios provides a clinically feasible approach to human imaging.

Key Words: kinetic modeling; numeric simulations; ^{18}F-glutamine; animal imaging; triple negative breast cancer

J Nucl Med 2021; 62:1154–1162
DOI: 10.2967/jnumed.120.250977

Malignant cells reprogram pathways of energy metabolism for accelerated growth (*1*), providing opportunities for imaging and targeted treatment. Dysregulated glucose metabolism has been leveraged for PET imaging with ^{18}F-FDG, a tracer that has shown broad clinical applicability, in clinical oncologic imaging (*2*). A growing body of research suggests that dysregulated cellular metabolism extends beyond increased glucose consumption (*3*). Complementary to glucose, cancers may consume glutamine, the most abundant amino acid in plasma (*4*). Glutamine has numerous cellular metabolic fates. It can serve as an alternative energy substrate to glucose and as a source for building carbon skeletons and for nitrogen metabolism and biosynthesis (*5–8*). Numerous oncogenes and tumor suppressor genes have been implicated in the control of glutamine metabolism, most notably upregulation of the *MYC* oncogene (*7*).

Oncogene-dependent reliance on glutamine is a cancer vulnerability that has been exploited for therapeutic gain. The first step in glutaminolysis, conversion of glutamine to glutamate via the glutaminase enzyme, represents a prime target to inhibit the entire pathway, and several inhibitors have been developed (*9–11*). The glutaminase inhibitor CB-839 (Calithera Biosciences) has demonstrated antiproliferative activity in cell lines with accelerated glutamine metabolism, including triple-negative breast cancer (TNBC) cell lines (*11*,*12*). Sensitivity of breast cancer cell lines to CB-839 correlated with glutaminase activity and baseline glutamate-to-glutamine cellular concentration ratio, an indirect measure of glutaminase activity (*11*,*12*). The generally increased glutaminase activity and susceptibility of TNBC to CB-839 has supported clinical trials of this agent in patients with TNBC. In both treatment-naïve and pretreated cohorts, partial responses were achieved in some, but not all, patients (*13*,*14*). The variable activity of CB-839 between cell lines and nonuniform radiologic response in TNBC patients suggests a need for a biomarker to predict and monitor CB-839 efficacy. Cellular studies suggest that glutamine pool size at baseline and after CB-839 could be used as a surrogate to measure cellular glutamine metabolism (*11*,*12*) and, by extension, serve as a biomarker for targeted glutaminase therapy.

Received Jun. 5, 2020; revision accepted Oct. 19, 2020.
For correspondence, contact Varsha Viswanath (varsha.viswanath@pennmedicine.upenn.edu).
Published online December 4, 2020.

The PET radiotracer ^{18}F-(2*S*,4*R*)4-fluoroglutamine (^{18}F-Gln) has been developed as an in vivo measure of tumor glutamine metabolism (*15*), and uptake has been seen in a variety of cancers (*16–19*). ^{18}F-Gln uses the same cellular transporters as native glutamine but is minimally metabolized (*12*,*17*,*20*). In cell uptake studies and early animal data, ^{18}F-Gln generally washes out from cells over time, suggesting reversible transport (*12*,*20*). These properties make ^{18}F-Gln an ideal radiotracer for measuring glutamine pool size. Indeed, ^{18}F-Gln tumor-to-blood ratios demonstrated a strong positive correlation with glutamine pool size as measured by ^{1}H MR spectroscopy (*12*). However, the optimal method for PET image analysis has not been established for this experimental radiotracer. In this paper, we model the kinetics of ^{18}F-Gln observed in 2 breast cancer xenografts in mice, using both graphical and compartmental analyses to estimate parameters relevant to glutamine transport and cellular pool size. On the basis of our previously published preclinical data (*12*), we hypothesize that the distribution volume (V_D) of ^{18}F-Gln is a marker of tumor glutamine pool size that can be used to infer levels of tumor glutaminolysis. On the basis of the known biology of ^{18}F-Gln, a 2-compartment model with a small amount of trapping should best model the data. However, we hypothesize that the rate of trapping will be difficult to estimate, which in turn will affect the estimation of glutamine pool size, the kinetic parameter of interest. For quantification, computer simulations were used to study the mathematic properties of the model, with the goal of building a foundation for quantitative interpretation of ^{18}F-Gln in human studies.

MATERIALS AND METHODS

Mouse Models

Human breast cancer xenografts were established in mice as previously described (*12*). Briefly, xenografts from HCC1806 (TNBC cell line) and MCF-7 (receptor-positive breast cancer cell line) were implanted in NCR athymic *nu/nu* mice subcutaneously. The glutaminase activity in these cell lines has been shown to be high for the HCC1806 xenograft and low for the MCF-7 xenograft (*11*). Tumors were allowed to grow to an adequate size as measured by calipers on the skin before each PET scan (baseline, 270–1,057 mm^3; after treatment, 210–1,374 mm^3). The glutaminase inhibitor CB-839 was supplied through a generous material transfer agreement by Calithera Biosciences. CB-839 was dissolved in the vehicle solution and administered via oral gavage (200 mg/kg twice daily). Control mice received the same volume of vehicle solution without CB-839 added. Four to 6 doses of CB-839 or vehicle solution were administered. The posttreatment scan was performed at least 4 h after the last CB-839 administration to allow for adequate absorption. This short treatment course was given to ensure a metabolic effect of glutaminase inhibition without changes in overall tumor volume that could confound image interpretation, as documented in prior studies (*12*).

Six HCC1806 xenografts and 6 MCF-7 xenografts were analyzed. Each subtype includes 3 CB-839–treated and 3 vehicle solution–treated mice. Two mice were scanned at baseline and after vehicle solution treatment and then were subsequently treated with CB-839 and scanned. The post-vehicle treatment scan was used as the baseline for the post–CB-839 scan.

^{18}F-Gln Radiosynthesis

^{18}F-Gln was synthesized as previously described (*15*,*21*). Radiochemical purity was greater than 90%. Specific activity was greater than 4,847 MBq/mol; the detection limit was less than 5 μg/mL.

^{18}F-Gln PET Studies

A dedicated small-animal PET scanner was used for all studies (A-PET, a prototype of the Philips Mosaic HP; Philips, Amsterdam, NE), with technical parameters and performance characteristics as detailed previously (*22*). The spatial resolution is 2.3 mm, and the 3-dimensional row-action maximum-likelihood algorithm (*23*) was used for reconstruction into 1 mm^3 isotropic resolution. Images were decay-corrected; scatter and attenuation correction was not used, in view of the small size of a mouse. The mice were sedated during imaging via oxygen containing 1.5% isoflurane, inhaled through a nose cone at a rate of 1 L/min.

All mice were scanned using the following dynamic protocol. PET imaging was initiated immediately before a tail vein injection of 11.1–12.95 MBq (300–350 μCi) of ^{18}F-Gln. The first 10 min of dynamic imaging was performed in list mode and parsed into 15 frames (6×10 s, 9×60 s). The remaining 50 min of PET data were collected in sinogram mode in 10 frames of 300 s each.

^{18}F-Gln Imaging Analysis

MIM, version 6.7.10, was used to view PET images and draw volumes of interest (VOIs). To delineate VOIs for tumor time–activity curves, a search area was manually drawn on the last 5-min frame to include the tumor and exclude nearby structures with high physiologic uptake (e.g., liver). The location of the peak VOI found in MIM (i.e., a 16-voxel spheric VOI where the mean counts were maximized within the search area) was used to draw the VOI in MATLAB (The MathWorks), and time–activity curves were constructed from mean values in the VOI. This method of selecting the VOI was based on PERCIST (*24*) and adapted for mouse imaging while allowing us to exclude the photopenic centers of the tumors. Additionally, MATLAB appropriately weights voxels that are only partially covered by the spheric VOI. Time–activity curves were corrected for frame duration and scaled to units of percentage injected dose per gram as described in prior work by Zhou et al. (*12*). These measures were also used to calculate tumor-to-blood ratios.

Compartmental Model

A 2-compartment model with irreversible trapping and a single blood input was used (Fig. 1). K_1 denotes the transport rate constant from blood to tissue. k_2, the reverse of K_1, represents the rate constant of reversible transport from the tissue compartment back to blood. Lastly, k_3 represents the rate constant of tracer trapping, presumed to be due to the incorporation of tissue glutamine into macromolecules such as peptides. This model was based on observations that ^{18}F-Gln is transported into and out of cells similarly to glutamine but is minimally metabolized; therefore, the metabolite ^{18}F-glutamate is not included in the model, and the reversible compartment for ^{18}F-Gln is considered to reflect the cellular glutamine pool size. The hypothesis underlying our model is therefore that ^{18}F-Gln V_D in the reversible compartment provides an estimate of cellular glutamine concentration, which is the desired marker of glutaminase activity and inhibition. There is a possibility that a small fraction of ^{18}F-Gln is incorporated into macromolecules (*12*), indicating the need for a second compartment in the model and the parameter k_3 to account for this minor effect. k_3 is denoted with a dashed arrow in the model. In a 2-compartment model, the V_D of the reversible compartment is $V_D = K_1/(k_2+k_3)$. For a

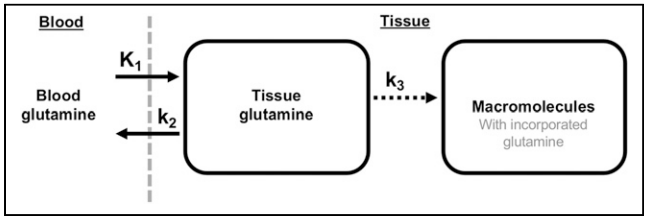

FIGURE 1. Proposed compartment model of ^{18}F-Gln.

single-compartment model (i.e., setting $k_3 = 0$), the V_D equation reverts to $V_D = K_1/k_2$.

We previously noted some prior reports of ^{18}F-Gln–to–^{18}F-glutamate metabolism. Gas chromatography–mass spectroscopy cellular studies reported that minimal metabolism of ^{19}F-glutamine was observed (*17*). ^{18}F-glutamate (8%–9% of total activity) was seen in the supernatant of mouse and rat tumor extracts on high-performance liquid chromatography analysis at 1 h (*20*). An alternative compartment model has been proposed for ^{18}F-Gln that hypothesizes significant metabolism of ^{18}F-Gln to ^{18}F-glutamate (*19*). Our prior studies on breast cancer mouse models demonstrated that at least 85% of the radioactivity in the supernatant of tumor tissue was in the form of ^{18}F-Gln and that only 9%–14% of activity was from metabolites (*12*). Much of the ^{18}F-glutamate may be related to blood metabolites that arise from degradative organs such as liver and kidney, as 82%–87% of blood radioactivity was in the form of ^{18}F-Gln and less than 16% was from metabolites (*12*). We therefore consider alternative models that include the possibility of tumor tissue metabolism to ^{18}F-glutamate as well as transport of ^{18}F-glutamate as a blood metabolite to tissue (Supplemental Fig. 1; supplemental materials are available at http://jnm.snmjournals.org). However, since metabolism of ^{18}F-Gln to ^{18}F-glutamate appears to be minimal in most reported studies, we focus our analysis largely on the model illustrated in Figure 1.

Kinetic Parameter Estimation

The tumor and blood time–activity curves derived above were input into PMOD, version 3.7 (PMOD Technologies, LLC). Image-derived arterial input functions served as the input to the model for all analyses, and raw data obtained from image analysis were fit empirically to a linear function until the peak of the input curve. After the peak, a sum of 3 exponentials was fit to the data as implemented in PMOD to reduce input noise, as has been performed in several other similar studies (*25*). For compartmental analysis, model parameters were estimated using the Levenberg–Marquardt least-squares minimization algorithm as implemented in PMOD. Graphical analysis of blood and tumor time–activity curves was performed using Patlak and Logan analyses (*26*,*27*), also as implemented in PMOD. For Logan plot analysis, V_D was estimated as the slope of the line of $\int(C_{plasma}\,dt)/C_{tissue}$ versus $\int(C_{tissue}\,dt)/C_{tissue}$, where C_{plasma} is the blood plasma TAC, C_{tissue} is the tumor TAC, and dt is the differential with respect to time.

Model Characterization: Sensitivity Function

To test the mathematic behavior of the model, we based our further analysis on idealized uptake curves from a representative TNBC mouse and a representative estrogen receptor–positive (ER+) mouse, each treated with CB-839. The Akaike information criterion as calculated by PMOD was used to compare compartmental models (*28*). To characterize the kinetic models and performance in parameter estimation, sensitivity functions were calculated for each parameter using PMOD. In addition, the parameter identifiability matrices were estimated to determine the ability to independently estimate parameters (K_1, K_1/k_2, and k_3) for the model (*29*).

Assessment of Parameter Estimation Performance Using Simulated Curves with Added Poisson Noise

To measure the precision and bias of estimated parameters, time–activity curves from each of the 2 representative mice were fit using a 1-compartment model, a reversible 2-compartment model, and an irreversible 2-compartment model in PMOD. Radioactive delay, frame duration, and decay were applied to the time–activity curves to calculate counts collected in the tumor, and Poisson noise was added to each datapoint to generate 1,000 noise realizations ($\lambda =$ counts, $\sigma = \sqrt{\lambda}$). These curves were fit in PMOD using the corresponding compartmental model to assess the robustness of kinetic parameter estimation.

We then extended the simulation to use measured kinetic parameters from all imaged mice. Parameters were input into Stella, a model integration program (version 1.9.1; ISEE Systems), to generate 250

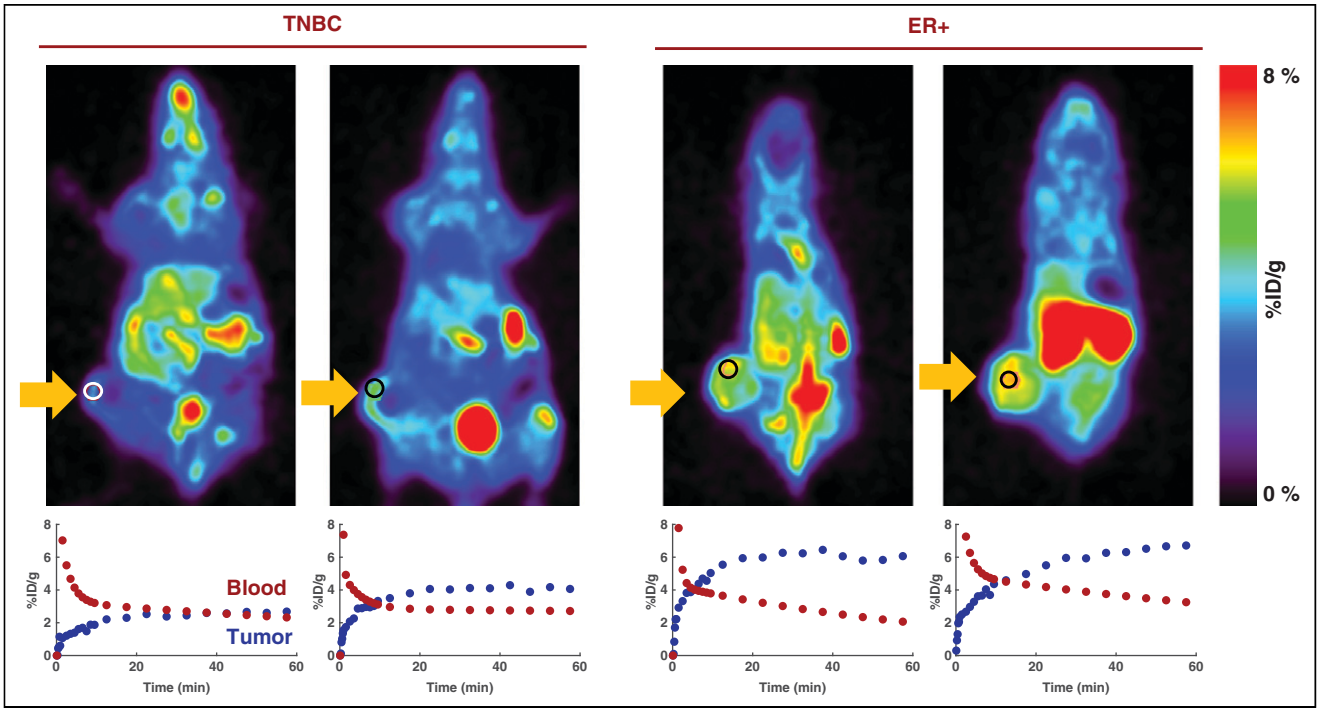

FIGURE 2. Static images of TNBC and ER+ tumor xenografts and response to glutaminase inhibition (post–CB-839 image is right-hand image of each pair). Tumor and blood time–activity curves demonstrate adequate temporal sampling of radiotracer uptake over time. Spheric VOIs used are drawn on each tumor. %ID = percentage injected dose.

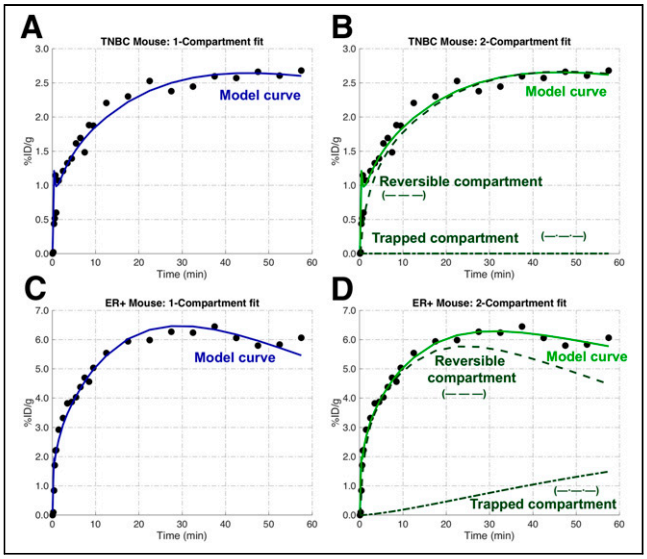

FIGURE 3. Single-compartment model fit (A and C) and double-compartment model fit (B and D) of same representative time–activity curves for ER+ and TNBC mice before treatment. Double-compartment fit separately shows time course of both reversible and trapped compartments. %ID = percentage injected dose.

time–activity curves for a 1-compartment model and an irreversible 2-compartment model. Poisson noise was added to these curves, as described above, to generate 100 noise realizations per curve, and all time–activity curves were fit in PMOD. Finally, to determine the effect of ignoring k_3 on V_D estimation, idealized curves from Stella were used to model a 2-compartment model with variable levels of trapping.

Statistical Analysis

Pearson correlation coefficients were calculated for pairwise comparisons between V_D estimates for each model. R^2 values were calculated to evaluate the fit of graphical analyses and the correlation between V_D for different models and tumor-to-blood ratios.

RESULTS

Blood and Tissue Time–Activity Curves

Representative blood and tissue time–activity curves are shown in Figure 2, along with the final frame imaged. At baseline, TNBC xenografts with inherently high glutaminase activity demonstrated low ^{18}F-Gln uptake compared with an ER+ xenograft with inherently low glutaminase activity (Fig. 2). On glutaminase inhibition with CB-839, there was increased radiotracer uptake in the TNBC tumor reflecting an increase in glutamine pool size, which was expected with the inhibition of glutaminolysis. In the ER+ tumor xenograft, only a minimal increase in radiotracer uptake was observed after glutaminase inhibition, reflecting known low glutaminase activity in this breast cancer subtype.

Compartmental Analysis of Xenograft Data

The 2 representative mice with typical time–activity curves (Fig. 2) were then selected for mathematic investigation of radiotracer uptake. Both a single-compartment model and a double-compartment model with trapping were investigated. The 1-compartment fit is shown in Figures 3A and 3C, and the 2-compartment fit is shown in Figures 3B and 3D. The blood fraction was fixed at 5% for these models and not estimated. A blood fraction of 5% is within the range of estimated values from a prior mouse xenograft study (*30*) and similar to the 4% blood fraction used in prior studies of ^{18}F-FDG in locally advanced breast cancer in humans (*31*).

The single-compartment model for the ER+ tumor underestimates ^{18}F-Gln uptake at later time points, unlike the 2-compartment model, which includes the possibility of retained tracer in a nonreversible compartment. The 2-compartment model estimates k_3 at 0/min for the TNBC mouse and 0.006/min for the ER+ mouse data, for which 27% of the total radioactivity is estimated to be contained in the nonreversible compartment at 60 min. This estimate is higher than the 10% ± 4% of radiotracer incorporated into the pellet versus supernatant of tumor extracts in prior work (*12*), perhaps because of the difficulty of estimating a small k_3, as supported by simulation data below. This finding, and the relatively low values of k_3 found across all animals studied, suggest that such a term could be omitted.

The Akaike information criterion of the TNBC mouse data fit using a single-compartment model was 60.9, more favorable than the 63.5 found using a 2-compartment model; the penalty of fitting an extra term in the 2-compartment model more than offset the slightly improved goodness of fit by the 2-compartment model. The Akaike information criteria for the ER+ tumor data fit using a single- and double-compartment model were nearly equal, at 34.4 and 33.8, respectively, noting the discrepancy between k_3 estimates for the 2-compartment model for ER+ tumors and measured data as described above. The benefits of omitting the second compartment are further supported by examining the accuracy and precision estimates of estimating k_3 as described below.

Graphical Analysis of Xenograft Data

Analyses using Patlak and Logan graphical approaches are shown in Figure 4. The Logan plots (Figs. 4A and 4C) demonstrated late linearity, consistent with minimal radiotracer trapping and largely reversible tracer exchange between the tumor and the blood. R^2 values for the fits of the TNBC and ER+ mouse data were 0.997 and 0.999, respectively, reflecting good-quality linear fits. In contrast, the Patlak plot demonstrates poor fits, arguing against irreversible radiotracer trapping; an R^2 of 0.91 and 0.83 for

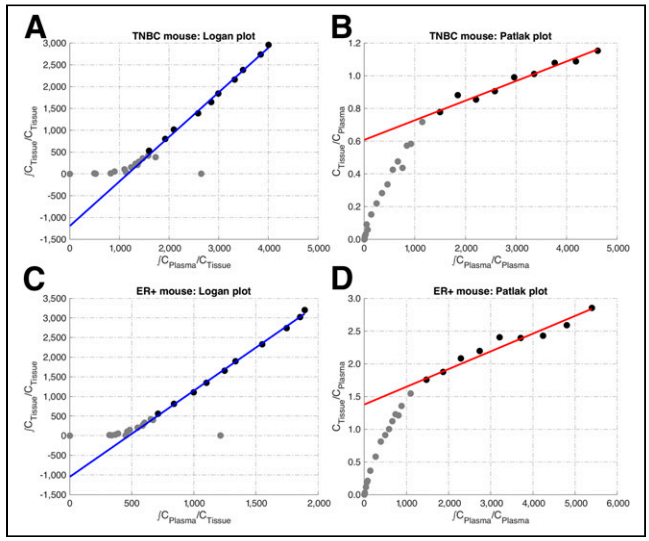

FIGURE 4. Logan graphical analysis (A and C) and Patlak graphical analysis (B and D) of same representative time–activity curves for ER+ and TNBC mice before treatment.

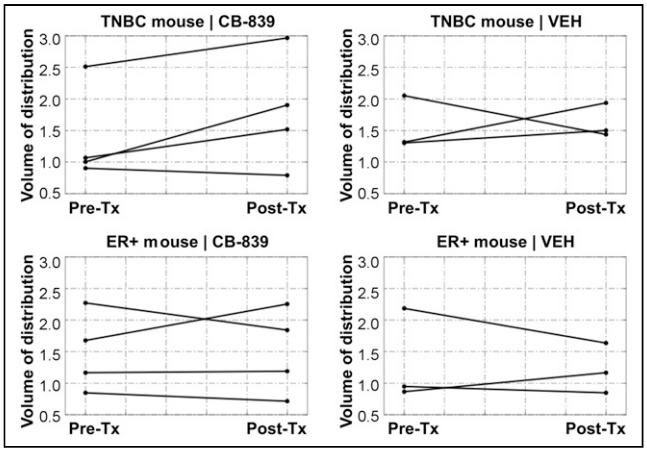

FIGURE 5. Changes in volume of distribution, as estimated by a 1-compartment model, for both TNBC and ER+ mice who underwent treatment of tumor xenografts with GLS inhibitor (left) or placebo (right). VEH = vehicle solution.

the TNBC and ER+ mouse data, respectively, was obtained using fewer data points than the Logan fit. Graphical analyses support the use of the V_D as calculated by the slope of the best fit line in the Logan graphical analysis as a measure of glutamine pool size. The applicability of Logan analysis is consistent with the suitable fits of the single-compartment model.

Model Characterization Sensitivity and Identifiability Analysis

The sensitivity function for the 2 mice fit using an irreversible 2-compartment model (Supplemental Fig. 2) suggests that both models are most sensitive to K_1 early after injection, more sensitive to K_1/k_2 at intermediate time points, and most sensitive to k_3 at late time points. The identifiability matrix (Supplemental Table 1) for the 2-compartment model suggests that K_1 and K_1/k_2 can be estimated independently but that K_1/k_2 and k_3 have a high covariance (-0.97) and cannot be estimated independently, suggesting that errors in k_3 estimation will propagate into V_D, and supports the exclusion of k_3 in the model.

Effect of Glutaminase Therapy on Volume of Distribution and Tumor-to-Blood Ratios

After glutaminase inhibition, V_D increased in TNBC xenografts, but not consistently in MCF-7 xenografts or vehicle solution–treated TNBC tumors (Fig. 5). Of the 4 TNBC tumors treated with CB-839, 3 had an increase in V_D (18%, 42%, and 89%), whereas 1 had a decrease after treatment. This study was not powered to detect an increase in V_D after glutaminase inhibition in any subgroup. One of the 4 mice had a baseline V_D markedly elevated above the others, indicative of less glutaminolysis and atypical of TNBC. Previously, we showed a 4.3-fold increase in glutamine pool size by MRS in TNBC xenografts after glutaminase inhibition. Given a 2.5-fold increase in plasma glutamine concentration with glutaminase inhibition, an increase in tumor-to-blood ratio and a V_D of 4.3/2.5 = 1.7 would be expected (*12*). Additionally, variability in PET signal response to CB-839 supports differential glutaminase inhibition in breast cancer subtypes and supports the need for a biomarker to measure glutamine metabolism.

Simulation of Parameter Estimation

Simulations (Fig. 6A) revealed that the precision and accuracy in recovering the true V_D was better for the 1-compartment model than for either 2-compartment model. The reversible 2-compartment model (Supplemental Fig. 1B) cannot accurately or precisely estimate V_D and was not further studied. The average bias in the median V_D and the %SD of the interquartile range (Supplemental Eq. 1) were markedly improved for the 1-compartment model compared with the irreversible 2-compartment model (bias, <0.5% vs. 1.6–12.9%; %SD, 7.73%–20.2% vs. 19.4%–54.3%), demonstrating the robustness of the 1-compartment model in contrast to the poor performance of the 2-compartment model.

Simulations that used kinetic parameters from all mice (Fig. 6B) clearly demonstrated more precise recovery of the true V_D when estimated using a 1-compartment model, in agreement with simulations in Figure 6A. The average %SD, calculated as %SD = SD/mean for each data point, was 9.7% ± 3.4% for the 1-compartment model and 33% ± 30% for the 2-compartment model with trapping.

The accuracy and precision of the individual recovered kinetic parameters (K_1 and k_3) in the simulations described above are shown in Supplemental Figure 3. K_1 was better estimated using the 1-compartment model. k_3 estimation with an irreversible 2-compartment model had a large bias and %SD, resulting in overestimation of activity in the trapped compartment (Fig. 3D). Additionally, errors in k_3 propagated to errors in V_D.

Comparison of V_D and Tumor-to-Blood Ratios

For all imaged mice, V_D estimates were compared with tumor-to-blood ratios (Fig. 7), which serve as a proxy of V_D obtained from static images, using the final time point. Strong correlations were seen between tumor-to-blood ratios versus V_D estimated by Logan plots or a single-compartment model but not a double-compartment model. This finding underscores the inaccuracy of using a 2-compartment model to estimate V_D and thus glutamine pool size.

Alternative Compartmental Models

We considered alternative compartmental models (Supplemental Figs. 1B and 1C) that included the possibility of reversible ^{18}F-Gln metabolism to ^{18}F-glutamate in tumor tissue. These models, specifically model 1B, were able to fit the data well, but nearly 50% of fits resulted in a near-zero k_4 or k_3, or a k_4 so large (~8 min^{-1}) that the ratio of k_3/k_4, the V_D of ^{18}F-glutamate, is essentially zero. The other half of fits resulted in rates of washout from the reversible compartment (k_4 or $k_4 + k_5$) that were comparable in magnitude to the k_3 metabolism rate (i.e., $k_3/k_4 = 1.06 \pm 1.08$). This implies a small V_D for ^{18}F-glutamate comparable to ^{18}F-Gln; however, in the glutaminolytic TNBC cells, ^{18}F-glutamate would be retained in a large intracellular pool of glutamate in cells actively metabolizing glutamine to glutamate (*11*,*32*). Liquid chromatography–tandem mass spectrometry studies on HCC-1806 TNBC tumors demonstrated a tumor glutamate concentration approximately 5 times greater than the tumor glutamine concentration (*11*), implying that the V_D of glutamate (i.e., k_3/k_4) should be 5 times the V_D of glutamine (5–10 mL/cm^3, given a glutamine V_D of 1–2 mL/cm^3). Thus, models that include finite tumor metabolism of ^{18}F-Gln to ^{18}F-glutamate do not appear to fit the observed tracer kinetic data in the mouse models and the known high concentration of glutamate in glutaminolytic cells.

We also tested a model that included transport of ^{18}F-glutamate, as a labeled metabolite in the blood, to tumor tissue (Supplemental Fig. 1D). We divided the arterial input curve into principal components of ^{18}F-Gln and ^{18}F-Glu based on sampled blood data (*12*).

We estimated K_1' and k_2' (glutamate kinetic parameters) at 10% of their respective glutamine counterparts (K_1 and k_2). As shown in Supplemental Figure 4, the contribution of PET signal from tissue ^{18}F-Glu was largely linear over time and accounted for a small component of the total PET signal at later time points. This small ^{18}F-Glu component (8%) could account for underestimates of the model curve of a single-compartment model at later time points. The relatively small contribution of glutamate suggests that it can likely be ignored, particularly at earlier time points.

DISCUSSION

Our study provides a theoretic framework for kinetic analysis of ^{18}F-Gln in mouse xenografts of human breast cancer. Previous work showed a linear relationship between ^{18}F-Gln tumor-to-blood ratios and tumor glutamine concentration and demonstrated an increase in glutamine pool size after targeted glutaminase inhibition of TNBC mice but not ER+ mice (*12*). On the basis of radiotracer biology, a 2-compartment irreversible model should fit the data well; however, the small value of k_3 is difficult to estimate accurately and leads to spurious estimates of V_D of ^{18}F-Gln. Thus, a 1-compartment model is favored and correlates well with changes in glutamine pool size after glutaminase inhibition. The distinctive kinetics of ^{18}F-Gln necessitate specific model and image analysis approaches distinct from those used for other cancer tracers such as ^{18}F-FDG (*33*), and this paper establishes a new imaging paradigm for this novel radiotracer that is now being used in several clinical trials.

We first demonstrated that dynamic time–activity curves and the images recapitulated the previously described patterns of uptake (*12*). That is, ^{18}F-Gln uptake late after injection was lower in

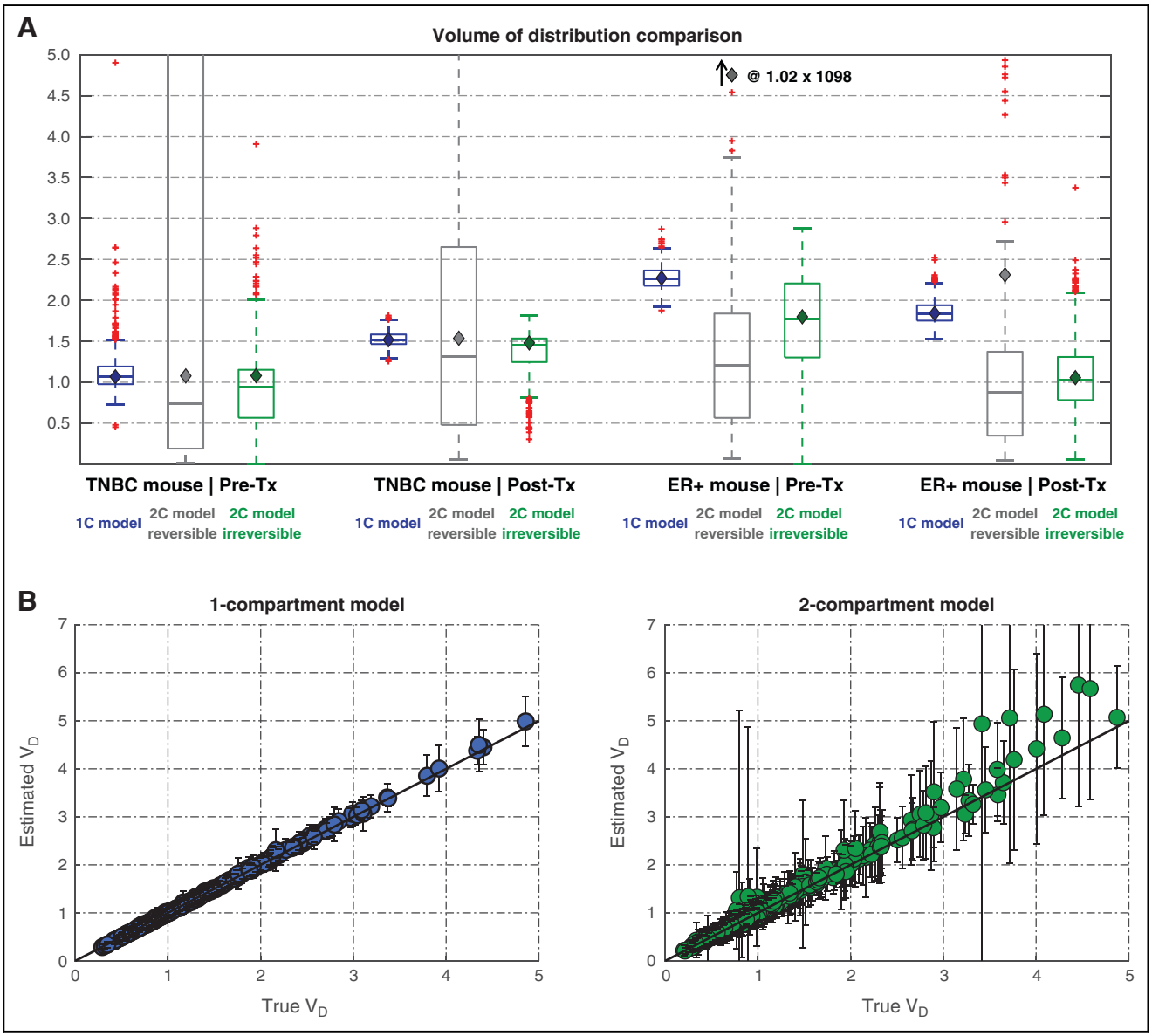

FIGURE 6. (A) Comparison of estimation of volume of distribution for 1- and 2-compartment models after adding Poisson noise to time–activity curves and fitting each noise realization with corresponding model. Boxes reflects 25th, 50th, and 75th percentiles of data, and whiskers are extent of data after outlier removal (1.5 × interquartile range, where interquartile range = 75th–25th percentiles). Diamonds show true V_D before noise is added to fit curve. True value for ER+ mouse before treatment is essentially infinite because of near-zero k_4. (B) Comparison of true vs. estimated V_D for 1- and 2-compartment models with trapping, where diagonal line is line of identity. 1C = 1-compartment; 2C = 2-compartment.

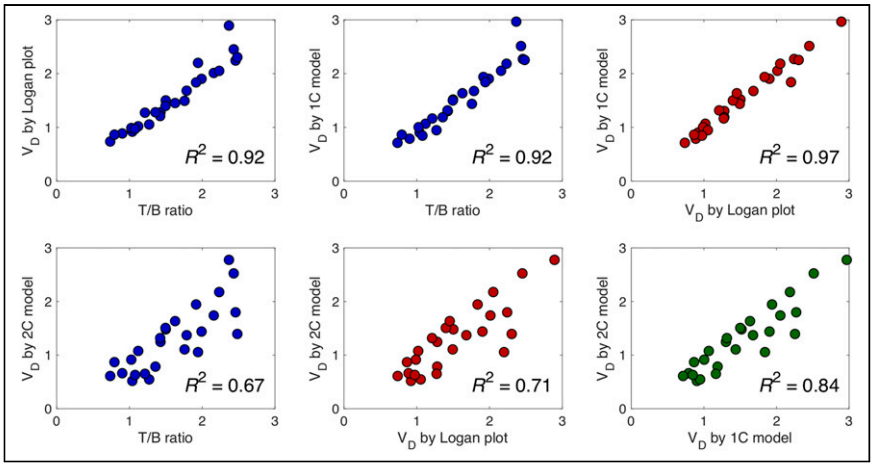

FIGURE 7. Comparison of volume of distribution of ^{18}F-Gln by compartmental and graphical analysis, as well as tumor-to-blood ratios. 1C = 1-compartment; 2C = 2-compartment.

TNBC than ER+ models, inversely related to glutaminase activity in those cell lines (*11*). ^{18}F-Gln uptake increased in the highly glutaminolytic tumor (TNBC) after glutaminase inhibition but not in the low-glutaminase ER+ lines (*12*). This behavior was accurately captured by the ^{18}F-Gln V_D, which estimates the cellular glutamine pool size, supporting the utility of this measure as a pharmacodynamic measure of glutaminase inhibitor therapy.

On the basis of the biochemistry of glutamine and the imaging analog, ^{18}F-Gln, a 1-compartment reversible model and a 2-compartment irreversible model were investigated in 2 representative mice. The second compartment in the 2-compartment model represents incorporation of ^{18}F-Gln into macromolecules, likely peptides. The 2-compartment model overestimated the percentage of radiotracer incorporated into macromolecules in an ER+ mouse compared with data from prior tumor extract studies (*12*), suggesting error in estimating k_3. The TNBC model, with inherently high glutaminase expression, had negligible trapping. Sensitivity analysis of the 2-tissue-compartment model with irreversible trapping demonstrated relative insensitivity of the model to k_3, other than late after injection, suggesting that this parameter could not be estimated accurately (Supplemental Fig. 2). Simulations provided additional support for omitting k_3 from the final model. Graphical analysis supported the use of a reversible model, in this case the single-compartment model. Thus, analysis of xenograft model data, model performance characteristics, and model simulations support the use of a 1-compartment model to estimate the key ^{18}F-Gln parameter, V_D.

The strong correlation between tumor-to-blood ratios and V_D of a single-compartment model and slope of a Logan plot (Fig. 7) suggests that static protocols could be considered for human imaging and should be a focus of early human studies. However, ignoring tracer trapping in the 1-compartment model could bias V_D estimation for modest levels of trapping, as shown in simulation without added noise (Supplemental Fig. 5). This bias can be mitigated by imaging at earlier time points (e.g., 20–30 min), which should be examined in human imaging studies.

Our proposed model and results are consistent with other preclinical and early clinical studies. Schulte et al. showed that the pharmacologic inhibition of glutamine transport in a TNBC mouse model resulted in reduced early uptake and decreased late retention, with kinetics consistent with our 1-compartment model (*34*). ^{18}F-Gln-PET has been explored as a measure of glutamine metabolism in early clinical trials. ^{18}F-Gln uptake was seen in a variety of cancers: paraganglioma, breast, colon, lung, pancreas, neuroendocrine, glioma, and thyroid (*16–19*). Downsloping time–activity curves in these human tumors support reversible kinetics. Preliminary analysis of a patient from this trial demonstrated the plausibility of a 1-compartment model based on good agreement of V_D between the Logan fit and the 1-compartment fit (Supplemental Fig. 6). The application of the framework established here in mouse xenografts can be applied to human ^{18}F-Gln imaging. Although the biology in human tumors may vary from the mouse xenografts and warrants use of a slightly altered kinetic model, the methodologies developed in this paper will permit testing of these hypotheses (*16*). Further analysis of human studies is warranted.

We examined alternative compartment models that included the possibility of tumor metabolism of ^{18}F-Gln to ^{18}F-glutamate suggested by others (*19*), based on observation of defluorination of ^{18}F-Gln in human studies (*16*) and some enzymatic studies demonstrating metabolism of ^{18}F-Gln to ^{18}F-glutamate (*35*). Although these models were able to fit our mouse data, the estimated parameters grossly underestimated the size of the tumor glutamate pool, as measured in prior studies, including our studies in TNBC mouse models (*11*,*12*). It is possible that kinetics differ in humans, although our early human data show a good fit for our 1-compartment model (Supplemental Fig. 6). We also examined the small impact of labeled metabolites, which may explain the inability of the 1-compartment model to fit the later portion of some observed curves. This impact on the estimate of ^{18}F-Gln V_D appears to be small but should be studied carefully in human data.

There are several limitations to broad application of this small-animal imaging study. Although 2 cell lines were used in this study, we believe these results are generalizable to other cell lines given the mechanism of uptake and lack of metabolism of the radiotracer. Subcutaneously implanted tumors may have intrinsic biologic properties different from those of human breast tumors, precluding direct translation. For example, cellularity is not a factor in mouse xenografts but may complicate the interpretation of V_D in humans, possibly necessitating a normalization factor. Future studies using other cell lines (especially TNBC), mouse models, and human imaging should address these limitations.

VOI analysis of mouse images varies greatly across studies, but our method, which was based on PERCIST, was designed to reproducibly draw a spheric VOI over the tumor. Our method ensured that the search area would not erroneously cover the mouse liver or knee and that the photopenic center of the tumor would not be included in the VOI. Time–activity curves were then scaled to percentage injected dose per gram using the total counts in the final image, as opposed to the total injected dose. Although this method is not standard, it does not affect our results since both the blood and the tumor time–activity curves are image-derived and thus similarly scaled for kinetic analysis. Additionally, we fit the image-derived blood time–activity curve to a triexponential to reduce noise, as is typical for human imaging, as opposed to direct

blood sampling of the mouse. The image-derived blood curve is more representative of human imaging and better represents estimation of V_D in human trials.

Mouse imaging estimates of time–activity curves are less accurate than human time–activity curves, partly because of differences in uptake, especially for estimates of the blood input function. An image-derived blood input function was used without metabolite correction. Minimal metabolism of ^{18}F-Gln in the blood supports such an input function (*12*), though others have used corrected input functions (*19*,*36*). Peripheral metabolism of ^{18}F-Gln to ^{18}F-glutamate may further confound the interpretation of ^{18}F-Gln uptake in tumors, but as noted, the effect appears to be small and may be able to be ignored, particularly at earlier time points. Finally, our modeling work is specific to ^{18}F-Gln and cannot be applied to ^{11}C-Gln, which has a much more complex kinetic model and is under preliminary investigation (*37*).

Our compartment model assumed no tumor metabolism of ^{18}F-Gln to ^{18}F-glutamate, based on our prior mouse model studies (*12*). However, on the basis of the defluorination of ^{18}F-Gln observed in human studies (*16*), as well as some enzymatic studies demonstrating metabolism of ^{18}F-Gln to ^{18}F-glutamate (*36*), other groups have hypothesized that there might be tumor metabolism of ^{18}F-Gln by glutaminase and proposed a 2-compartment reversible model (Supplemental Fig. 1B) (*19*). However, parameter estimates obtained from the model with 2 reversible compartments were not compatible with the large glutamate pool size observed in glutaminolytic tumors by a variety of methods (*11*,*12*,*32*). Rapid metabolism of ^{18}F-glutamate by alanine aminotransferase with resultant defluorination and efflux of the label from the tumor cell (Supplemental Fig. 1C) (*19*,*35*) also yields estimates of glutamate pool size that are much smaller than reported and therefore thought to be a less likely explanation for the observed kinetics.

CONCLUSION

This work found ^{18}F-Gln uptake in breast xenograft models to be largely reversible, consistent with the hypothesis that ^{18}F-Gln exchanges with the intracellular glutamine pool. Using a combination of traditional modeling and simulations, we determined that a 1-compartment model best estimated V_D and that robust estimates of V_D can also be found using Logan graphical analysis or tumor-to-blood ratios at 60 min after injection. This study establishes a theoretic framework for analyzing further human ^{18}F-Gln-PET imaging studies, which have recently begun. The pairing of ^{18}F-Gln with glutaminase inhibitors to select and monitor oncologic patients represents a prime opportunity to use molecular imaging to guide metabolically targeted cancer therapy.

DISCLOSURE

Work presented here is partially supported by the following grants: NIH KL2-TR001879, NIH R01-CA211337, Susan G. Komen SAC130060, and NIH R21-CA198563. Calithera provided CB-839. No other potential conflict of interest relevant to this article was reported.

ACKNOWLEDGMENTS

We thank Eric Blankmeyer for assisting with animal imaging and Tiffany Rodriguez for analyzing the human imaging study.

KEY POINTS

QUESTION: What kinetic model best estimates the uptake of ^{18}F-Gln dynamic data and captures relevant biology?

PERTINENT FINDINGS: A 1-compartment model accurately and precisely estimated the V_D of ^{18}F-Gln, a proxy for glutamine pool size. Other models were less robust and did not reflect known glutamine biology.

IMPLICATIONS FOR PATIENT CARE: The V_D from a 1-compartment model captures relevant glutamine biology and will be studied in ongoing clinical studies of ^{18}F-Gln in human breast cancer.

REFERENCES

1. Hanahan D, Weinberg RA. Hallmarks of cancer: the next generation. *Cell.* 2011;144:646–674.
2. Jacques L, Jensen TS, Rollins J, Caplan S, Roche JC. Decision memo for positron emission tomography (FDG) for solid tumors (CAG-00181R4). Centers for Medicare and Medicaid Services website. https://www.cms.gov/medicare-coverage-database/details/nca-decision-memo.aspx?NCAId=263. Published June 11, 2013. Accessed March 10, 2021.
3. Pantel AR, Ackerman D, Lee S-C, Mankoff DA, Gade TP. Imaging cancer metabolism: underlying biology and emerging strategies. *J Nucl Med.* 2018;59:1340–1349.
4. DeBerardinis RJ, Cheng T. Q's next: the diverse functions of glutamine in metabolism, cell biology and cancer. *Oncogene.* 2010;29:313–324.
5. Hensley CT, Wasti AT, DeBerardinis RJ. Glutamine and cancer: cell biology, physiology, and clinical opportunities. *J Clin Invest.* 2013;123:3678–3684.
6. DeBerardinis RJ, Lum JJ, Hatzivassiliou G, Thompson CB. The biology of cancer: metabolic reprogramming fuels cell growth and proliferation. *Cell Metab.* 2008;7:11–20.
7. Altman BJ, Stine ZE, Dang CV. From Krebs to clinic: glutamine metabolism to cancer therapy. *Nat Rev Cancer.* 2016;16:619–634.
8. Wise DR, Thompson CB. Glutamine addiction: a new therapeutic target in cancer. *Trends Biochem Sci.* 2010;35:427–433.
9. Robinson MM, McBryant SJ, Tsukamoto T, et al. Novel mechanism of inhibition of rat kidney-type glutaminase by bis-2-(5-phenylacetamido-1,2,4-thiadiazol-2-yl)ethyl sulfide (BPTES). *Biochem J.* 2007;406:407–414.
10. Wang JB, Erickson JW, Fuji R, et al. Targeting mitochondrial glutaminase activity inhibits oncogenic transformation. *Cancer Cell.* 2010;18:207–219.
11. Gross MI, Demo SD, Dennison JB, et al. Antitumor activity of the glutaminase inhibitor CB-839 in triple-negative breast cancer. *Mol Cancer Ther.* 2014;13:890–901.
12. Zhou R, Pantel AR, Li S, et al. [^{18}F](2S, 4R) 4-fluoroglutamine PET detects glutamine pool size changes in triple-negative breast cancer in response to glutaminase inhibition. *Cancer Res.* 2017;77:1476–1484.
13. Vidula N, Bardia A. Targeted therapy for metastatic triple negative breast cancer: the next frontier in precision oncology. *Oncotarget.* 2017;8:106167–106168.
14. Vidal G, Kalinsky K, Stringer-Reasor E, et al. Efficacy and safety of CB-839, a small molecule inhibitor of glutaminase, in combination with paclitaxel in patients with advanced triple negative breast cancer (TNBC): initial findings from a multicenter, open-label phase 2 study [abstract]. *Cancer Res.* 2019;79(suppl):P6-20-07.
15. Qu W, Zha Z, Ploessl K, et al. Synthesis of optically pure 4-fluoro-glutamines as potential metabolic imaging agents for tumors. *J Am Chem Soc.* 2011;133:1122–1133.
16. Dunphy MP, Harding JJ, Venneti S, et al. In vivo PET assay of tumor glutamine flux and metabolism: in-human trial of ^{18}F-(2*S*,4*R*)-4-fluoroglutamine. *Radiology.* 2018;287:667–675.
17. Venneti S, Dunphy MP, Zhang H, et al. Glutamine-based PET imaging facilitates enhanced metabolic evaluation of gliomas in vivo. *Sci Transl Med.* 2015;7:274ra17.
18. Xu X, Zhu H, Liu F, et al. Dynamic PET/CT imaging of ^{18}F-(2*S*, 4*R*)4-fluoroglutamine in healthy volunteers and oncological patients. *Eur J Nucl Med Mol Imaging.* 2020;47:2280–2292.
19. Grkovski M, Goel R, Krebs S, et al. Pharmacokinetic assessment of ^{18}F-(2*S*,4*R*)-4-fluoroglutamine in patients with cancer. *J Nucl Med.* 2020;61:357–366.
20. Lieberman BP, Ploessl K, Wang L, et al. PET imaging of glutaminolysis in tumors by ^{18}F-(*2S,4R*) 4-fluoroglutamine. *J Nucl Med.* 2011;52:1947–1955.

21. Li S, Schmitz A, Lee H, Mach RH. Automation of the radiosynthesis of six different ^{18}F-labeled radiotracers on the AllinOne. *EJNMMI Radiopharm Chem.* 2017;1:15.
22. Surti S, Karp JS, Perkins AE, et al. Imaging performance of A-PET: a small animal PET camera. *IEEE Trans Med Imaging.* 2005;24:844–852.
23. Daube-Witherspoon M, Matej S, Karp J, Lewitt R. Application of the row action maximum likelihood algorithm with spherical basis functions to clinical PET imaging. *IEEE Trans Nucl Sci.* 2001;48:24–30.
24. Wahl RL, Jacene H, Kasamon Y, Lodge MA. From RECIST to PERCIST: evolving considerations for PET response criteria in solid tumors. *J Nucl Med.* 2009;50(suppl):122S–150S.
25. Vriens D, de Geus-Oei L-F, Oyen WJ, Visser EP. A curve-fitting approach to estimate the arterial plasma input function for the assessment of glucose metabolic rate and response to treatment. *J Nucl Med.* 2009;50:1933–1939.
26. Logan J, Fowler JS, Volkow ND, et al. Graphical analysis of reversible radioligand binding from time–activity measurements applied to [*N*-^{11}C-methyl]-(−)-cocaine PET studies in human subjects. *J Cereb Blood Flow Metab.* 1990;10:740–747.
27. Patlak CS, Blasberg RG. Graphical evaluation of blood-to-brain transfer constants from multiple-time uptake data: generalizations. *J Cereb Blood Flow Metab.* 1985;5:584–590.
28. Akaike H. A new look at the statistical model identification. *IEEE Trans Automat Contr.* 1974;19:716–723.
29. Mankoff D, Muzi M, Zaidiy H. Quantitative Analysis in Nuclear Medicine Imaging. Springer; 2006:494–536.
30. Kim SJ, Lee JS, Im KC, et al. Kinetic modeling of 3′-deoxy-3′-^{18}F-fluorothymidine for quantitative cell proliferation imaging in subcutaneous tumor models in mice. *J Nucl Med.* 2008;49:2057–2066.
31. Tseng J, Dunnwald LK, Schubert EK, et al. ^{18}F-FDG kinetics in locally advanced breast cancer: correlation with tumor blood flow and changes in response to neoadjuvant chemotherapy. *J Nucl Med.* 2004;45:1829–1837.
32. Zhou R, Bagga P, Nath K, Hariharan H, Mankoff DA, Reddy R. Glutamate-weighted chemical exchange saturation transfer magnetic resonance imaging detects glutaminase inhibition in a mouse model of triple-negative breast cancer. *Cancer Res.* 2018;78:5521–5526.
33. Mankoff DA, Farwell MD, Clark AS, Pryma DA. Making molecular imaging a clinical tool for precision oncology: a review. *JAMA Oncol.* 2017;3:695–701.
34. Schulte ML, Fu A, Zhao P, et al. Pharmacological blockade of ASCT2-dependent glutamine transport leads to antitumor efficacy in preclinical models. *Nat Med.* 2018;24:194–202.
35. Cooper AJ, Krasnikov BF, Pinto JT, Kung HF, Li J, Ploessl K. Comparative enzymology of (2*S,4R*)4-fluoroglutamine and (2*S,4R*)4-fluoroglutamate. *Comp Biochem Physiol B Biochem Mol Biol.* 2012;163:108–120.
36. Miner MW, Liljenback H, Virta J, et al. (2*S,* 4*R*)-4-[^{18}F]fluoroglutamine for *in vivo* PET imaging of glioma xenografts in mice: an evaluation of multiple pharmacokinetic models. *Mol Imaging Biol.* 2020;22:969–978.
37. Padakanti P, Pantel AR, Choi H, et al. Refined analysis of [^{11}C]L-glutamine metabolism in triple negative breast cancer xenograft model. Abstract presented at: WIMC Virtual 2020, World Molecular Imaging; October 7–9, 2020.